Solar Physics (2024) 299:133
https://doi.org/10.1007/s11207-024-02378-9

RESEARCH

Characterizing High-Energy Solar Proton Events with Energies Below and Above 100 MeV

Dheyaa Ameri[1,2] · Eino Valtonen[2] · Amjad Al-Sawad[3] · Rami Vainio[2]

Received: 12 March 2024 / Accepted: 12 September 2024

Abstract

We analyzed 58 high-energy proton events that occurred during the years 1996 – 2022. In 32 out of the 58 (55%) events, the proton energies extended up to ∼ 68 MeV but did not reach 100 MeV. In the remaining 26 events, the proton energies exceeded 100 MeV. We studied the differences in the characteristics of these proton events and their associations with solar and interplanetary phenomena to improve understanding proton sources and acceleration processes.

The coronal mass ejections (CMEs) associated with > 100 MeV proton events appeared to be, on average, more energetic than those associated with < 100 MeV proton events. The peak and integrated fluxes (fluence) of the soft X-ray (SXR) flares were higher in > 100 MeV proton events, but there was almost no difference in the rise times of the flares. In a major part of the > 100 MeV proton events, protons were released over the rise phase of the SXR flares, whereas in most of the < 100 MeV events the proton releases occurred after the peak of the SXR flares. We established limits for the CME speed V_{CME} and SXR peak flux F_{pk} or total fluence F_i, which helped us to distinguish the events in the two groups. Solar eruptions with $V_{CME} > 1000$ km s^{-1} and $F_{pk} > 5 \cdot 10^{-5}$ W m^{-2} had a high probability to produce proton events of > 100 MeV. On the other hand, eruptions with $V_{CME} > 900$ km s^{-1} and $F_i < 5 \cdot 10^{-4}$ J m^{-2} and eruptions with $V_{CME} < 900$ km s^{-1} irrespective of the SXR total fluence were very likely to produce proton events of < 100 MeV.

All proton events were associated with decametric Type III radio bursts, and most of them had Type II bursts associations either in metric or decametric–hectometric (DH) wavelengths or both. Both metric- and DH-Type II emissions were observed in 50% of < 100 MeV proton events while they were observed in 88% of > 100 MeV events. Our analysis showed that protons in most of the > 100 MeV events were released low in the corona (≤ 3.0 R$_\odot$) before the onsets of the DH-Type II radio bursts. Conversely, protons in most of the < 100 MeV events were released higher in the corona (> 3 R$_\odot$) and after the DH-Type II onsets.

We conclude that protons in most of the > 100 MeV events are accelerated either by the flare reconnection processes or by shocks low in the corona and could undergo reacceleration higher in the corona in CME shocks manifested in DH-Type II radio emission. In the < 100 MeV events, protons are mainly accelerated in CME shocks at coronal heights > 3 R$_\odot$.

Keywords Solar proton events · Coronal mass ejections · Flares · Radio emissions

Extended author information available on the last page of the article

Published online: 25 September 2024

1. Introduction

Solar Energetic Particle (SEP) events, consisting of protons, electrons, and heavier nuclei, are accelerated at the Sun as well as in the interplanetary (IP) medium during the solar flares and/or coronal mass ejections (CMEs) and propagate along IP magnetic field lines from the Sun to the Earth (e.g., Cane, Richardson, and von Rosenvinge 2010; Papaioannou et al. 2016; Reames 2021, and references therein). A two-category paradigm, impulsive and gradual, has been used for classification of SEP events. The impulsive events are thought to be related to solar flares. They are electron-rich and associated with Type III radio bursts. In gradual events, particles are thought to be accelerated up to high energies in CME shocks. They are proton-rich and associated with Type II radio bursts (Reames 1999, 2013, 2021; Desai and Giacalone 2016). Impulsive SEP events result from resonant stochastic acceleration in magnetic reconnection regions, whereas gradual SEP events result from shock acceleration (e.g., Reames 2002).

The impulsive-gradual paradigm has been challenged by many observations. For example, in a recent statistical study, Papaioannou et al. (2016) found that most of the SEP events in their catalogue consisting of 314 SEP events did not conform to the simple two-category division. Some studies (e.g., Kocharov and Torsti 2002; Kallenrode 2003) have suggested mixed/hybrid models for SEP origins. SEP characteristics in these events may be similar to gradual events but may also show some properties of impulsive events (Vainio et al. 2007). In mixed/hybrid events, SEPs may result from reacceleration of seed particles from flares or seed particles produced by CME lift-off processes (Kocharov and Torsti 2002). It has also been suggested that in mixed/hybrid events, CMEs accelerate particles from the material of preceding CMEs rather than from the quiet solar wind (Gopalswamy et al. 2002).

Gopalswamy et al. (2012) studied SEPs at energies reaching 1 GeV in ground level enhancement (GLE) events of Solar Cycle 23 and their associated solar eruption properties. They found that the initial acceleration of the CMEs that produced GLE events was by a factor of two larger than that of the CMEs that did not produce GLE events. In another study, Gopalswamy et al. (2014) investigated the key factors affecting the occurrence of large SEP and GLE events. They suggested that the soft X-ray (SXR) flare is not a good indicator of SEP or GLE events, whereas the CME speed is, being consistently high in large SEP and GLE events and supporting the shock acceleration mechanism. Xie et al. (2019) found a strong correlation between the CME kinetic energy and SEP peak intensity, which they interpreted as a strong evidence for the CME-shock acceleration theory of SEPs.

Solar radio bursts play a significant role in the characteristics and occurrence of SEP events. Cliver, Kahler, and Reames (2004) found that 25% of the bursts observed only at metric wavelengths were associated with SEP events, whereas the association increased to $\sim 90\%$ when the metric-Type II bursts were accompanied by DH-Type II emission (see also Gopalswamy 2003; Gopalswamy et al. 2005). The study by Cliver and Ling (2009) revealed a high association rate (96%) between gradual SEP events and DH-Type II bursts, contrasting with a low association rate (5%) for impulsive events. Miteva et al. (2013) found that both gradual and impulsive SEP events are associated with Type III radio bursts, whereas they have a lower association with Type II.

Kouloumvakos et al. (2015) investigated the properties of SEP events related to different cases of radio bursts associations. They concluded that major proton events at over 50 MeV were consistent with both flare- and shock-related particle release processes. The study also concluded that distinguishing between flare-related and CME-related SEP events is complicated.

In a recent study, Ameri, Valtonen, and Pohjolainen (2019) divided the high-energy proton events into two categories: In Category 1 the protons were associated with only metric-Type II, or the proton release time occurred before the DH-Type II onset, whereas in Category 2 the protons were associated with only DH-Type II, or the proton release time occurred after the DH-Type II onset. The study concluded that acceleration of protons in Category 1 events occurred low in the corona, either by CME-driven shocks, or in solar flares, or in CME initiation-related processes, whereas the protons in Category 2 events were accelerated by CME-driven shocks high in the solar corona.

The purpose of the present investigation is to characterize two sets of proton events: one with energies extending up to ~ 68 MeV but not reaching 100 MeV, and the other with proton energies exceeding 100 MeV. Based on potential differences in their characteristics and associations with solar and interplanetary phenomena, we strive to improve the understanding of the proton sources and acceleration processes and to recognize conditions leading to proton energies exceeding 100 MeV. We investigate the characteristics of 58 high-energy proton events and their solar sources and associations with radio emissions. The data sources and the event selection are presented in Section 2. In Section 3, we describe the data analysis and the characterization of the proton events with energies below and above 100 MeV. The main results are summarized and discussed in Section 4, and the conclusions are presented in Section 5.

2. Data Sources

The high-energy ($\gtrsim 68$ MeV) proton events observed by the *Energetic and Relativistic Nuclei and Electron* (ERNE)[1] experiment (Torsti et al. 1995) on board the *Solar and Heliospheric Observatory* (SOHO) spacecraft (Domingo, Fleck, and Poland 1995) during the years 1996 – 2022 are used in this study. The high-energy detector of ERNE covers the proton energy range 13.8 – 131 MeV in ten differential energy channels. We also use proton data from the *Geostationary Operational Environmental Satellites* (GOES)[2] to identify events with proton energies exceeding 100 MeV. The CME catalog of the SOHO *Large Angle Spectroscopic Coronagraph* (LASCO)[3] (Brueckner et al. 1995) was used to find the CMEs associated with the proton events. For solar soft X-ray flares associated with the events, we used GOES[4] observations.

To understand the impact of the flare acceleration on particles in the upper corona, we checked the decametric-Type III radio bursts observed by Wind/Plasma and Radio Waves (WAVES)[5] (Bougeret et al. 1995). To understand the coronal shocks traced in metric (m) Type II radio bursts and in decahectometric (DH) Type II radio bursts, we used the radio burst onset times given in the major SEP event list[6] of the CDAW Data Center and the CDAW catalog[7] for CME-associated Type II radio bursts constructed by Gopalswamy, Mäkelä, and Yashiro (2019). For event dates with no reported m-Type II bursts in the list of

[1] srl.utu.fi/erne_data/.

[2] www.ngdc.noaa.gov/stp/satellite/goes/dataaccess.html.

[3] cdaw.gsfc.nasa.gov/CME_list.

[4] hesperia.gsfc.nasa.gov/goes/goes_event_listings/.

[5] cdaw.gsfc.nasa.gov/images/wind/waves/.

[6] cdaw.gsfc.nasa.gov/CME_list/sepe/.

[7] cdaw.gsfc.nasa.gov/CME_list/radio/waves_type2.html.

the CDAW Data Center, we further checked the radio dynamic spectra provided by Hiraiso Radio Spectrograph (HiRAS),[8] Green Bank Solar Radio Burst Spectrometer (GBSRBS),[9] Learmonth solar observatory (LEAR) and Culgoora solar radio spectrograph (CULG).[10]

We used the online catalog[11] of Paassilta et al. (2017) for preliminary identification of proton events. This catalog consists of high-energy proton events observed by ERNE at energies 55 – 80 MeV (nominal energy $\sim$ 68 MeV) during the years 1996 – 2022. However, for this investigation, we selected events only from solar longitudes E30° – W90° with a few events just behind the western solar limb. We also required that for the selected events, the path lengths of protons obtained from the velocity dispersion analysis (VDA), as explained in Section 3, were in the range 1 – 3 AU.

3. Data Analysis and Event Characterization

We performed velocity dispersion analysis for all proton events in the list of Paassilta et al. (2017) using 1-minute average proton intensities in eight energy channels of ERNE in the energy range 13.8 – 80.2 MeV. VDA is based on the linear relationship between the onset times of the particle intensities in different energy ranges at the observation site close to the Earth and the corresponding inverse speeds of the particles. We performed VDA using the same technique as Ameri, Valtonen, and Pohjolainen (2019) by applying the Poisson-CUSUM procedure (Huttunen-Heikinmaa, Valtonen, and Laitinen 2005) for determining the onset times and estimating their uncertainties by a bootstrapping method. The linear fit was performed using the Williamson–York method (Williamson 1968; York et al. 2004). For more detail, see Ameri, Valtonen, and Pohjolainen (2019). VDA gives an estimate of the solar release time of the particles at the acceleration site close to the Sun and the apparent path length traveled by the particles when propagating from the Sun to the Earth (see, e.g., Vainio et al. 2013). We further restricted our events by requiring that the apparent path length given by VDA was in the range $\sim$ 1 – 3 AU, since it has been shown that in this path length range, the corresponding release times of particles given by VDA are most reliable (Lintunen and Vainio 2004; Kahler and Ragot 2006; Vainio et al. 2013; Xie et al. 2016). We identified 74 high-energy proton events fulfilling our selection criteria. However, during 16 of the 74 events, SOHO was at 180° roll attitude, which means that ERNE was looking 45° east from the Sun–Earth line instead of the nominal interplanetary magnetic field line direction (45° west). In this case, ERNE does not observe unscattered particles, which leads to unknown inaccuracies in derived particle release times. Therefore we excluded these events from the analysis and were left with 58 events. These events with their associated soft X-ray flares, coronal mass ejections, and radio emissions are listed in Table 2 in the Appendix.

We divided the 58 SEP events in two groups with proton energies E $<$ 100 MeV and E $>$ 100 MeV. The proton intensities from ERNE/HED available for $<$ 100 MeV are used for the first group. For identifying E $>$ 100 MeV events, all ERNE/HED proton energy channels are used. Furthermore, we used the corrected 5-minute average fluxes of the differential proton channel P7 (165 – 500 MeV) and the integral channel P7 ($>$ 100 MeV) of GOES(8-12)/EPS for confirming E $>$ 100 MeV events. For dates after 2010, when EPS data were not available,

[8] solobs.nict.go.jp/radio/cgi-bin/MainDisplay.pl.

[9] www.astro.umd.edu/~white/gb/index.shtml.

[10] www.sws.bom.gov.au/World_Data_Centre/1/9.

[11] swe.ssa.esa.int/utu-srl-federated.

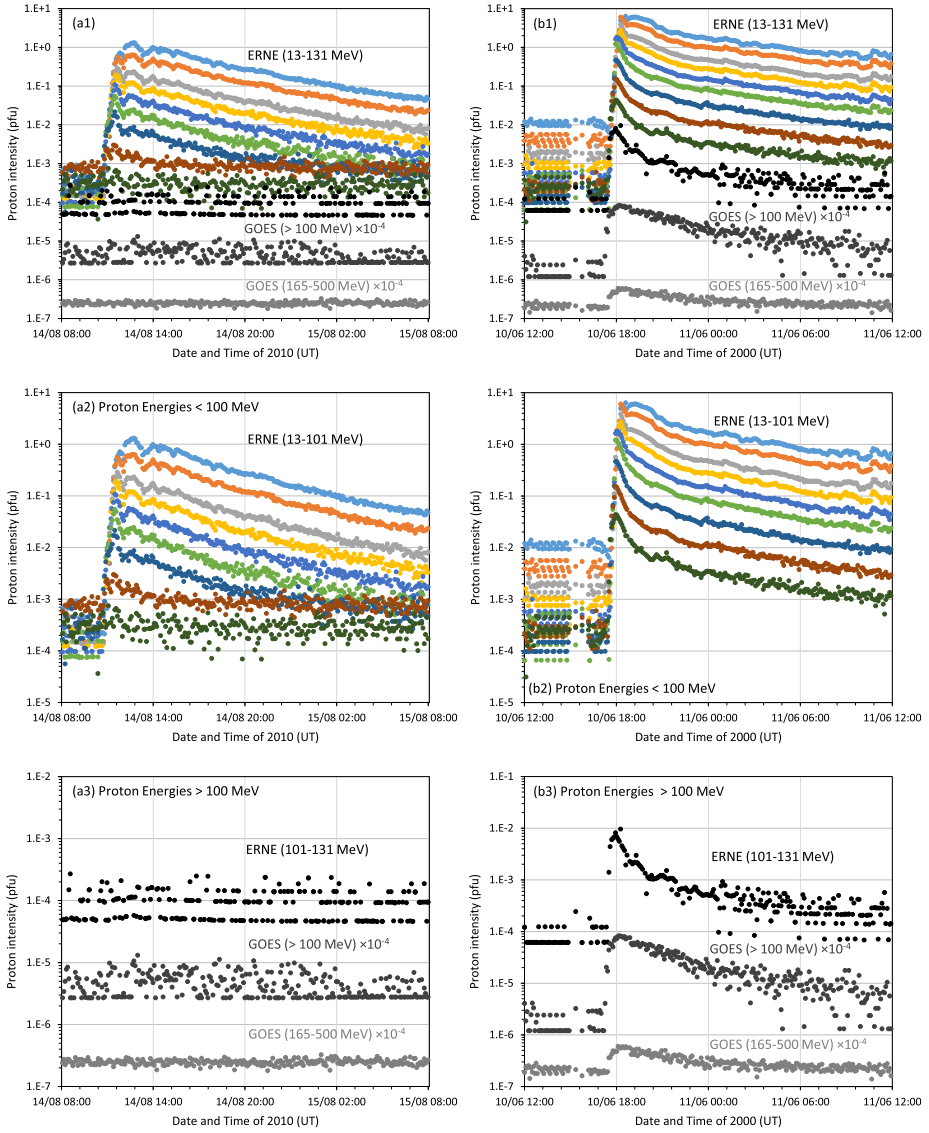

Figure 1 (a1) The temporal variations of proton intensities in ten energy channels of ERNE/HED along with the integral channel > 100 MeV and differential channel 165 – 500 MeV of GOES in the event of 14 August 2010 and (b1) the event of 10 June 2000. The ranges of the energy channels of ERNE/HED from top to bottom are (13.8 – 16.9), (16.9 – 22.4), (20.8 – 28.0), (25.9 – 32.2), (32.2 – 40.5), (40.5 – 50.8), (50.8 – 67.3), (63.8 – 80.2), (80.2 – 101), and (101 – 131) MeV. (a2), (b2) and (a3), (b3) are the same as (a1), (b1) but for proton energies < 100 MeV and > 100 MeV, respectively.

we used the corresponding energy channels from GOES(13-16)/EPEAD. Examples of both types of proton events are shown in Figures 1a (E < 100 MeV) and 1b (E > 100 MeV). In our set of events, 32 out of the 58 events (55%) belonged to the group E < 100 MeV, and the rest 26 (45%) in the group E > 100 MeV. We examined the characteristics of the events in these two groups to comprehend under which conditions particles can be accelerated to

energies > 100 MeV. The study focused on the observed characteristics of the SEP events, occurrence and timing of concomitant solar phenomena, and characteristics of the potential sources of the accelerated particles.

3.1. Time-Intensity Profiles and Energy Spectra of Protons

Figures 1a and 1b show the temporal profiles for the events of 14 August 2010 (E < 100 MeV) and 10 June 2000 (E > 100 MeV). For the first event. the increase in the intensity was detected up to 63.8 – 80.2 MeV as shown in Figure 1 (a2), whereas there was no enhancement of intensities above the background at energies > 100 MeV (see Figure 1 (a3)). For the second event the intensity increases were clearly detected at energies > 100 MeV as shown in Figure 1 (b2) and (b3).

We investigated the proton peak intensities, intensity rise times, and rise rates at two energy channels, 13.8 – 22.4 MeV (nominal energy 17.5 MeV) and 50.8 – 80.2 MeV (nominal energy 63.9 MeV). For E < 100 MeV events, the average peak intensity was 0.53 ± 0.13 pfu (1 pfu = 1 proton/(cm^2 s sr MeV)) at 17.5 MeV and 0.007 ± 0.001 pfu at 63.9 MeV, whereas for E > 100 MeV events, the corresponding peak intensities were 3.24 ± 0.53 pfu and 0.178 ± 0.034 pfu. These values demonstrate a significant difference in the efficiency of the acceleration mechanism in E < 100 MeV and E > 100 MeV events. For E < 100 MeV events, the efficiency is not only weaker, but also more rapidly decaying with energy.

To investigate the intensity rise time, we determined the onset times of the events using the same method as for VDA. The maximum intensities of the events were chosen to be near the end of the main rise phase to reduce the effects of possible fluctuations in the intensities and to exclude energetic storm particles. There was no significant difference in the average rise times of E < 100 MeV and E > 100 MeV proton events (see Table 1).

It is well known that the temporal profiles of SEP events originating from different solar longitudes (heliolongitudes) show differences in their intensities. To some extent, such longitude effects are attenuated for our events, since they were selected from the longitude range E30° to W90°, including four events lying behind the west limb. Most of the events originated from western longitudes, whilst only four events from both groups originated from the eastern longitudes. For all events, we determined the connection angle (see, e.g., Paassilta et al. 2017), i.e., the longitudinal distance of the flare site from the footpoint of the Parker spiral leading to the spacecraft near 1 AU. The connection angle is defined to be positive when the flare is located to the west from the footpoint and negative if the flare is to the east. For E < 100 MeV events, the connection angle ranged from 54° to −90° with 59% having negative connection angles. The range of the connection angles for E > 100 MeV was from 50° to − 76° being negative in 58% of the events. The average flare longitude and connection angle did not differ significantly between the two groups of events as shown in Table 1.

We calculated the intensity rise rate as the difference between the logarithms of the background-normalized intensity at 80% and 20% of the maximum divided by the corresponding rise time (see Equation 3 of Ameri, Valtonen, and Pohjolainen 2019). The average rise rate for E > 100 MeV events at the nominal energy ∼ 17.5 MeV was only slightly higher than that for E < 100 MeV events, whereas at the nominal energy ∼ 63.9 MeV, there was a significant difference. The rise rate for E > 100 MeV events was 0.044 ± 0.006 min^{-1}, and for E < 100 MeV events, only 0.019 ± 0.004 min^{-1}. This follows from the similar rise times of the events in the two groups but much higher peak intensities of E > 100 MeV events, which is emphasized at the higher energy. The results are summarized in Table 1.

Table 1 Average values with standard errors of the parameters characterizing the proton events in the two groups and the associated coronal mass ejections, soft X-ray flares, and radio emissions.

Parameter	E < 100 MeV events	E > 100 MeV events	p-value*
Proton events			
I_{pk} at 17.5 MeV (pfu)	0.53 ± 0.13	3.24 ± 0.53	$4.3 \cdot 10^{-5}$
I_{pk} at 63.9 MeV (pfu)	0.007 ± 0.001	0.178 ± 0.034	$5.6 \cdot 10^{-5}$
Rise time at 17.5 MeV (h)	2.07 ± 0.31	1.83 ± 0.22	0.52
Rise time at 63.9 MeV (h)	1.46 ± 0.24	1.56 ± 0.24	0.78
Rise rate at 17.5 MeV (min^{-1})	0.024 ± 0.003	0.029 ± 0.003	0.2
Rise rate at 63.9 MeV (min^{-1})	0.019 ± 0.004	0.044 ± 0.006	0.0012
Connection angle (°)	-16 ± 6	-11 ± 7	0.63
Spectral index	-2.95 ± 0.14	-2.10 ± 0.06	$1.4 \cdot 10^{-6}$
Path length (AU)	1.41 ± 0.06	1.64 ± 0.11	0.088
$t_{o,p} - t_{xro}$ (min)	37 ± 4	22 ± 3	0.0034
$t_{o,p} - t_{xrpk}$ (min)	18 ± 3	4 ± 3	0.0005
$t_{o,p} - t_{III}$ (min)	28 ± 4	12 ± 3	$6.1 \cdot 10^{-4}$
$t_{o,p} - t_{mII}$ (min)	27 ± 4	12 ± 3	0.0046
$t_{o,p} - t_{DHII}$ (min)	25 ± 4	-8 ± 4	$3.0 \cdot 10^{-7}$
Release height ($R_\odot$)	4.6 ± 0.4	3.2 ± 0.3	0.0066
Coronal mass ejections			
Linear speed ($km\,s^{-1}$)	1017 ± 85	1398 ± 99	0.006
Space speed ($km\,s^{-1}$)	1296 ± 92	1598 ± 117	0.063
Halo CME (%)	45	80	...
Angular width (°)	248 ± 21	329 ± 13	0.002
Initial acceleration ($km\,s^{-2}$)	1.35 ± 0.17	1.96 ± 0.23	0.056
Soft X-ray flares			
Peak flux (10^{-4} $W\,m^{-2}$)	0.61 ± 0.13	2.68 ± 0.85	0.023
Fluence (10^{-3} $J\,m^{-2}$)	1.13 ± 0.23	4.03 ± 1.16	0.021
Longitude (°)	44 ± 6	45 ± 7	~ 1
Rise time (min)	19 ± 2	18 ± 3	0.6
Duration (min)	40 ± 6	39 ± 6	0.88
Radio emissions			
Type III association (%)	100	100	...
m-Type II association (%)	78	92	...
DH-Type II association (%)	63	96	...
$t_{III} - t_{xrpk}$ (min)	-12 ± 2	-9 ± 1	0.2
$t_{mII} - t_{xrpk}$ (min)	-9 ± 2	-9 ± 2	~ 1
$t_{DHII} - t_{xrpk}$ (min)	-3 ± 2	11 ± 3	0.0027
Type mII onset height ($R_\odot$)	2.1 ± 0.2	2.1 ± 0.2	~ 1
Type DHII onset height ($R_\odot$)	3.1 ± 0.2	4.4 ± 0.4	0.01

* p-value of the null hypothesis that the averages of the two groups are equal derived from the two-tailed t-test

The symbols used in the table are:

I_{pk}: proton peak intensity, $t_{o,p}$: proton release time, t_{xro}: SXR flare onset, t_{xrpk}: SXR flare peak time, t_{III}: decametric Type III onset, t_{mII}: metric-Type II onset, and t_{DHII}: DH-Type II onset

We constructed single-power-law differential energy spectra of the form $I_{pk}(E) \propto E^{\gamma}$ in the energy range 13.8 – 80.2 MeV for the events of the two groups. The spectra were calculated by using the background-subtracted intensities at the time of the maximum (TOM; see, e.g., Van Hollebeke, Ma Sung, and McDonald (1975), Miroshnichenko (1996)) intensity using 1-hour integration time in most cases. For some events, a shorter integration time was used due to a rapid fall of the intensities after maximum. The spectral indices were derived by fitting a straight line for the log-log presentation of the intensities vs. energies using the Williamson–York fitting method (Section 2). For events 21, 27, and 58, a single power law was not a satisfactory fit, so they were excluded when calculating the average spectral index for E > 100 MeV events. For E < 100 MeV events, the range of spectral indices lay between -1.52 and -4.40 with the average of -2.95 ± 0.14. For E > 100 MeV events, the range was from -1.65 to -2.75 with the average of -2.10 ± 0.06. For 72% of the E < 100 MeV events, the spectral index was ≤ -2.5, whereas 87% of the E > 100 MeV events had the spectral index > -2.5.

3.2. Coronal Mass Ejections and Soft X-ray Flares

As the properties of the CMEs associated with the proton events, we investigated the CME linear speed V_{CME} and width given in the LASCO CME catalog (Yashiro et al. 2004), CME space speed, and CME initial acceleration. For two events, LASCO CME data were not available due to data gaps. The space speed for halo CMEs is given in the LASCO halo CME catalog (Gopalswamy et al. 2010). For nonhalo CMEs (width > 100°), we estimated the space speed by using the cone model of Xie, Ofman, and Lawrence (2004) and the formula given by Gopalswamy et al. (2010). We also estimated the CME initial acceleration based on the indirect flare-proxy method of Zhang et al. (2001) (see also Zhang and Dere 2006) by dividing the CME space speed by the rise time of the associated soft X-ray flare.

The CME linear speed of E < 100 MeV events ranged from 464 km s^{-1} to 2331 km s^{-1} being $\geq$ 900 km s^{-1} for half (16/31) of the events. For E > 100 MeV events, the range of speeds was from 546 km s^{-1} to 2459 km s^{-1} being for most of the events (22/25, 88%) $\geq$ 900 km s^{-1}. On average the CMEs associated with E > 100 MeV proton events were significantly faster than those associated with E < 100 MeV events as shown in Table 1. About half (55%) of the CMEs associated with E < 100 MeV events were nonhalos with an average width of 155° ± 19°. Only 20% of the E > 100 MeV CMEs were nonhalos and had the average width of 206° ± 14°. Average widths taking into account also the halo CMEs are given in Table 1. The average initial CME acceleration for E > 100 MeV events of 1.96 ± 0.23 km s^{-2} was found to be significantly higher than that of the E < 100 MeV events (1.35 ± 0.17 km s^{-2}).

To describe the characteristics of the solar soft X-ray flares, we used the longitude, peak flux F_{pk}, integrated flux (fluence) F_i, flare onset, rise and peak times, and flare duration. The results are noted in Table 1. We examined the time profiles of soft X-ray fluxes of all the flares. When several flares occur in quick succession, they merge together, and the onset times recorded in the GOES list are not accurate (Gopalswamy et al. 2012). For these cases, the onset times of the flares associated with the particle events are our estimates, and they deviate from those given in the GOES list. These events are marked with an asterisk in Table 2 in the Appendix. Only the average flare peak flux and fluence turned out to be significantly different between the E < 100 MeV and E > 100 MeV events. The range of soft X-ray peak flux for E > 100 MeV events was from M1.4 to X17, being for most (77%) of the events $\geq$ M5.0, whereas for E < 100 MeV, the range was from C3.2 to X3.7, being < M5.0 for 59% of the events. The averages of peak flux and fluence for E > 100 MeV events

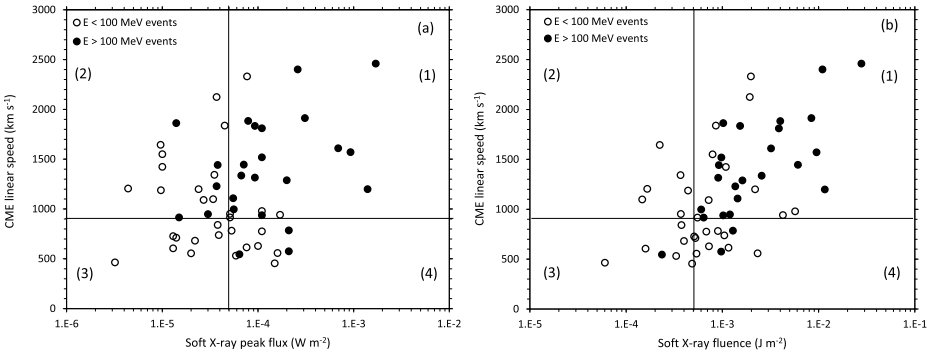

Figure 2 (a) Scatter plot of the CME linear speeds as functions of soft X-ray peak fluxes. (b) The same as (a) but as functions of soft X-ray total fluence for E < 100 MeV and E > 100 MeV events.

were $F_{pk} = (2.44 \pm 0.84) \cdot 10^{-4}$ W m^{-2} and $F_i = (4.03 \pm 1.16) \cdot 10^{-3}$ J m^{-2}, respectively, which were significantly higher than those of the E < 100 MeV events ($F_{pk} = (0.61 \pm 0.13) \cdot 10^{-4}$ W m^{-2} and $F_i = (1.13 \pm 0.23) \cdot 10^{-3}$ J m^{-2}).

To distinguish the E < 100 MeV and E > 100 MeV events from each other based on the CME and flare properties, we plotted the CME linear speeds as functions of the soft X-ray peak fluxes and total fluence for the two groups of events as shown in Figures 2a and 2b, respectively. In Figure 2 the horizontal lines are drawn at $V_{CME} = 900$ km s^{-1}, and the vertical lines at $F_{pk} = 5 \cdot 10^{-5}$ W m^{-2} (M5.0) (Figure 2a) and at $F_i = 5 \cdot 10^{-4}$ J m^{-2} (Figure 2b). These lines divide the proton events into four quadrants. In each quadrant the events are associated with different types of CME-flare combinations: quadrant (1) fast CMEs and strong flares, quadrant (2) fast CMEs and weak flares, quadrant (3) slow CMEs and weak flares, and quadrant (4) slow CMEs and strong flares. As shown by Figure 2, most of the E > 100 MeV events are in quadrant (1) in both Figures 2a and 2b: 17 out of 25 (68,%) in Figure 2a and 22 out of 25 (88%) in Figure 2b. None of the E > 100 MeV events is in quadrant (3) of Figure 2a (slow CME and weak flare peak flux), and none in quadrant (2) of Figure 2b (fast CME and low flare fluence). Only one of the E > 100 MeV events is in quadrant (3) of Figure 2b and two in quadrant (4). However, E < 100 MeV events are quite evenly distributed in all quadrants of Figure 2b with 10 events in quadrant (1), which makes it impossible to reliably distinguish E > 100 MeV events. On the other hand, CME speeds below 900 km s^{-1} with any value of soft X-ray fluence and CME speeds above 900 km s^{-1} with F_i below $5 \cdot 10^{-4}$ J m^{-2} are quite reliable signatures of E < 100 MeV events (Figure 2b). Using soft X-ray peak flux does not improve the separation between the two groups of proton events, although increasing the CME speed limit in this case to 1000 km s^{-1} would leave only one E < 100 MeV event against 15 E > 100 MeV events in our data set in quadrant (1) of Figure 2a, making the conditions $V_{CME} > 1000$ km s^{-1} and $F_{pk} > 5 \cdot 10^{-5}$ W m^{-2} a reliable signature of E > 100 MeV events. However, a significant amount of E > 100 MeV events also falls below these limits ($V_{CME} = 1000$ km s^{-1} and $F_{pk} = 5 \cdot 10^{-5}$ W m^{-2}).

3.3. Type II and III Radio Emissions and Temporal Relations with Soft X-ray Flares

We consider the onset times of radio emissions to be the times of their first appearance in the available dynamic radio spectra. We list both metric- and DH-Type II bursts for those events where the metric bursts seem to continue to DH wavelengths; the onset times are those of

the first appearance within the observed frequency ranges. The start time of a decametric-Type III burst is specifically determined as the highest frequency observed in Wind/WAVES RAD2 1-minute time resolution dynamic spectra, typically at 14 MHz. A radio burst is considered to be associated with a proton event if its onset time occurs after the start of a CME-associated flare.

All the 58 high-energy proton events investigated were associated with decametric-Type III bursts. Almost all, 29/32 (91%), E < 100 MeV events and all E > 100 MeV events were also associated with Type II bursts either in metric or DH wavelengths or both. Both metric- and DH-Type II emissions were observed in 16 (50,%) E < 100 MeV events, whereas metric- only and DH-Type II only were observed in 9 (28%) and 4 (13%) events, respectively. For E > 100 MeV events, both metric- and DH-Type II bursts were associated with 23 (88%) events, whereas only metric-Type II and only DH-Type II were observed in one (4%) and two (8%) events, respectively.

The onset times of the decametric-Type III radio bursts (t_{III}) occurred in most cases (91%) of both event groups over the rise phase of the SXR flare, i.e., during the time from the onset (t_{xro}) to the peak flux (t_{xrpk}) of the SXR flare. The onsets of the metric-Type II bursts (t_{mII}) over the rise phase of the SXR flare were found to occur slightly more frequently, in 92% of the E < 100 MeV events and in 96% of the E > 100 MeV events. The average time differences $t_{III} - t_{xrpk}$ and $t_{mII} - t_{xrpk}$ were similar for the two groups of events, as shown in Table 1. For DH-Type II bursts, the finding was different. For E < 100 MeV events, the DH-Type II onset (t_{DHII}) occurred in most cases (12/20, 60%) over the rise phase of the SXR flare, whereas for E > 100 MeV events, it occurred in most cases (21/25, 84%) after the SXR rise phase. The range of $t_{DHII} - t_{xrpk}$ was from − 51 min to 12 min for E < 100 MeV events and from − 20 min to 53 min for E > 100 MeV events. The average time differences, -3 ± 2 min for E < 100 MeV and 11 ± 3 min for E > 100 MeV events, were significantly different.

3.4. Proton Release Times with Respect to Soft X-ray Flares and Radio Emissions

The release times of protons ($t_{o,p}$) were derived using the velocity dispersion analysis as described in Section 3. The distributions of the time differences $t_{o,p} - t_{xrpk}$ are shown in Figure 3a. These distributions are based on the nominal values of $t_{o,p}$ without taking into account their uncertainties presented in Table 2 in the Appendix. When investigating the proton release times of the two groups of events with respect to the peak time of the SXR flares, we found that in most of the E < 100 MeV events (26/32, 81%), the release times were consistent with the proton release occurring after the SXR peak time. In the major part (15/26, 58%) of the E > 100 MeV events, protons were released over the rise phase. On average, the time differences between the proton release times and the SXR peak or onset times were significantly shorter for E > 100 MeV events compared to E < 100 MeV events (Table 1).

Protons in all events were released over or after the type III radio burst onsets, with the exception of event number 15 (E > 100 MeV). The same was true for the metric-Type II onsets with two exceptions (events number 21 (E > 100 MeV) and 30 (E < 100 MeV)). The distributions of the differences between the nominal proton release times and the decametric-Type III ($t_{o,p} - t_{III}$) and metric-Type II ($t_{o,p} - t_{mII}$) onsets are heavily overlapping for the two groups of proton events (Figures 3b and 3c), but mainly due to the longer tails of the E < 100 MeV events, the average time differences for E < 100 MeV events were significantly longer than those for the E > 100 MeV events (Table 1).

For DH-Type II radio bursts, we found a significant difference between the E < 100 MeV and E > 100 MeV events, as shown in Figure 3d. Most of the E < 100 MeV events (17/20,

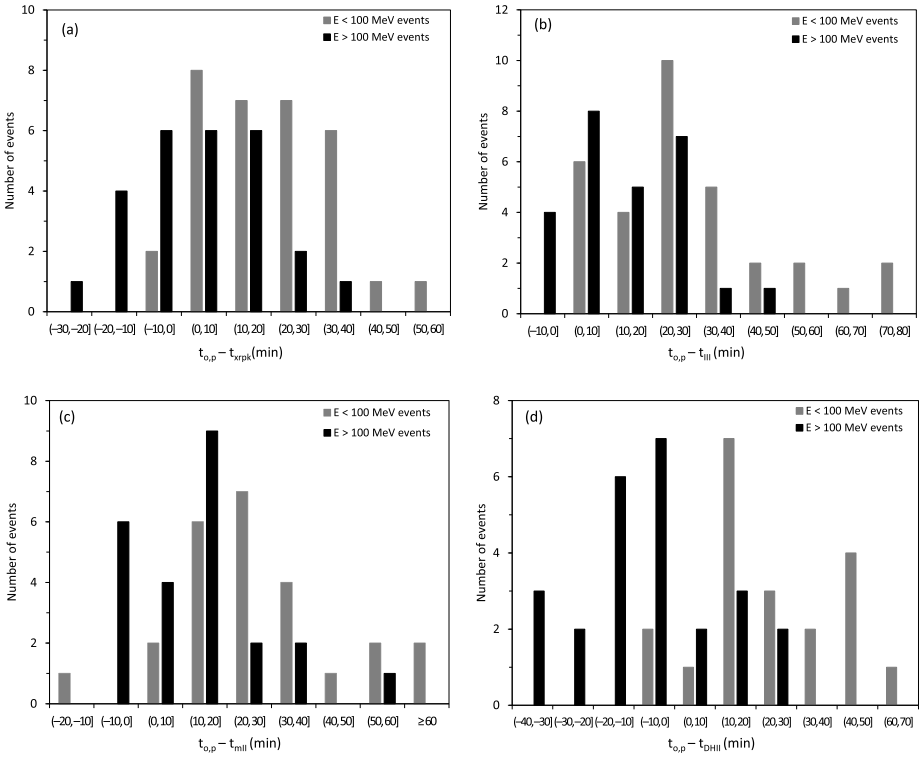

Figure 3 (a) Distributions of the differences between the proton release times and the peak times of the associated SXR flares for < 100 MeV and > 100 MeV proton events. (b) Distributions of the differences between the proton release times and the associated decametric-Type III onsets. (c) and (d) Distributions of the differences between the proton release times and the metric- and DH-Type II onsets. All distributions are based on the nominal proton release times.

85%) were released after the DH-Type II onset, whereas most of the E > 100 MeV events (20/25, 80%) were released before the onset. The average time difference between the proton release times and DH-Type II onsets ($t_{o,p} - t_{DHII}$) was -8 ± 4 min for E > 100 MeV events, which is significantly shorter than for E < 100 MeV events (25 ± 4 min).

3.5. Proton Release and Solar Radio Burst Heights

We estimated the proton release heights from the CME heights under the assumption that protons are accelerated in CME-driven shocks (Reames 2009). We used the height-time data given in the SOHO/LASCO CME catalog for the CMEs associated with our events. For two events, LASCO data were not available due to data gaps. When necessary, we extrapolated the heights downward using a simple linear fit (Yashiro et al. 2004). The release height of protons was assumed to be the height at which the leading front of the CME was at the proton release time as obtained from VDA. An additional assumption intrinsic to this method is that acceleration occurs in a shock close to the leading front of the CME, which can cause significant error in the obtained heights, if, e.g., the shock occurs on the CME flanks.

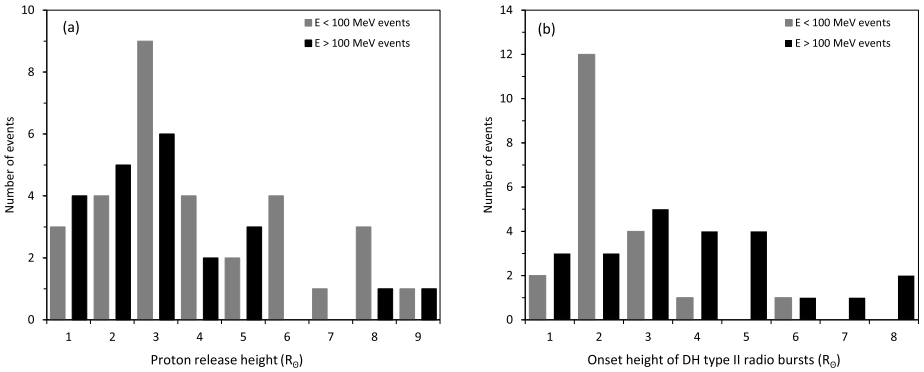

Figure 4 Distributions of the estimated heights for (a) the proton release and (b) the onset of DH-Type II radio bursts for E < 100 MeV and E > 100 MeV events based on the CME height-time data. In the proton release heights, the uncertainties in the proton release times are not taken into account.

Histograms of the proton release heights for the two groups of events are presented in Figure 4a. The range of proton release heights for E < 100 MeV events is from 1.5 $R_\odot$ to 9.8 $R_\odot$ with an average of 4.6 ± 0.4 $R_\odot$. For E > 100 MeV events, the main range is from 1.0 $R_\odot$ to 5.4 $R_\odot$. For three events, the result was < 1.0 $R_\odot$, which is clearly wrong. In addition, there were two isolated events with heights > 8 $R_\odot$. The average, calculated without the three events with heights < 1 $R_\odot$ and the two isolated outlier events at large heights, is 3.2 ± 0.3 $R_\odot$. Within the uncertainties caused by the uncertainties in the proton release times, most of the release heights of the E > 100 MeV events (16/25, 64%) are ≤ 3 $R_\odot$, whereas for 21 of the 31 (68%) E < 100 MeV events, the release heights are > 3 $R_\odot$. There is a significant overlap in the proton release heights between the two groups, as shown in Figure 4a. However, the two-tailed t-test shows that the average proton release heights are significantly different between the two groups.

We also estimated the onset heights of metric- and DH-Type II radio bursts based on the CME heights at the time of the onsets of these bursts (e.g., Gopalswamy et al. 2012). For almost all events, the onset heights of metric-Type II bursts were below 3.0 $R_\odot$. Event number 12 (E < 100 MeV) and events number 2 and 34 (E > 100 MeV) were exceptions, with heights being slightly above 3 $R_\odot$. For metric-Type II bursts, the average onset heights are similar for the two groups as presented in Table 1. The onset heights of the DH-Type II bursts were significantly different for the two groups of events as shown in Figure 4b. For a major part of the E < 100 MeV events (14/20, 70%), the DH-Type II onset heights were in the range from 1.0 to 3.0 $R_\odot$. For most of the E > 100 MeV events (17/24, 71%), DH-Type II onsets occurred at heights 3.3 – 8.8 $R_\odot$. For E > 100 MeV events, the average DH-Type II onset height was 4.4 ± 0.4 $R_\odot$, which is significantly higher than the corresponding height (3.0 ± 0.2 $R_\odot$) for E < 100 MeV events.

Comparing the DH-Type II onset heights and the proton release heights, we can conclude that proton events of > 100 MeV were released low in the corona before the DH-Type II onset, whereas proton events of < 100 MeV were released higher in the corona than the DH-Type II onset. This is consistent with the release times of protons relative to the onset times of DH-Type II bursts (see Section 3.4).

4. Summary and Discussion

We have analyzed high-energy proton events observed by SOHO/ERNE and the associated flares, CMEs and radio emissions. We used the online proton event catalog of Paassilta et al. (2017) and performed velocity dispersion analysis for the events in the energy range 13.8 – 80.2 MeV to determine the release times and apparent path lengths of the particles. For further analysis, we selected 58 proton events with apparent path lengths in the range 1.0 – 3.0 AU. An additional selection criterion was that the events originated from the longitude range E30° to W90°, with four events being behind the western limb. We divided the events into two groups based on the observed energy, E $<$ 100 MeV and E $>$ 100 MeV. We then investigated the characteristics of the events of these two groups with the aim to reveal under which prerequisites and circumstances particles are accelerated to energies exceeding 100 MeV. We also searched for signatures based on electromagnetic observations that could be used as a warning of such high-energy proton events. The results are summarized in Table 1.

The particle event characteristics that we investigated were the peak intensities, intensity rise times, and rise rates at the nominal energies 17.5 MeV and 63.9 MeV, energy spectra, connection angles, and release times and heights of the particles. In addition to certain temporal relations discussed later, there were significant differences between the E $<$ 100 MeV and E $>$ 100 MeV events in the peak intensities, rise rates, and spectral indices. The average peak intensities in E $>$ 100 MeV events at 17.5 MeV were by a factor of 6 times higher than in E $<$ 100 MeV events and at 63.9 MeV even by a factor of 25 (Table 1). The average rise rates at 17.5 MeV were similar but were by a factor of 2 higher at 63.9 MeV for E $>$ 100 MeV events. The average single power-law spectral index for E $<$ 100 MeV events was -2.95 ± 0.14, whereas for E $>$ 100 MeV, it was -2.10 ± 0.06. Kouloumvakos et al. (2015) found that the proton events associated with Type III/II radio bursts had significantly higher peak intensities and harder energy spectra than those associated with only Type III or only Type II bursts. The peak intensities and energy spectra of E $>$ 100 MeV events are similar to the Type III/II-associated events of Kouloumvakos et al. (2015). Also the average spectral index of E $>$ 100 MeV events is closer to the GLE events investigated by Gopalswamy et al. (2016), whereas the average spectral index of E $<$ 100 MeV events resembles that of the regular SEP events of Gopalswamy et al. (2016). The differences in the peak intensities, rise rates, and spectral indices of E $<$ 100 MeV and E $>$ 100 MeV events suggest that the efficiency of the acceleration mechanism for E $<$ 100 MeV events is not only weaker, but also more rapidly decaying with energy than for E $>$ 100 MeV events.

Eighty percent of the CMEs associated with E $>$ 100 MeV events were halos, whereas only 45% of the E $<$ 100 MeV events were associated with halo CMEs. Consequently, also the average angular width of all CMEs was significantly larger for E $>$ 100 MeV events. The average linear speed of the CMEs associated with E $>$ 100 MeV events was significantly higher (by a factor of 1.4) compared to E $<$ 100 MeV. Thus, on average, CMEs associated with E $>$ 100 MeV events are more energetic. Similarly, Firoz et al. (2010, 2011b) have observed that very high-energy solar particles producing GLEs are associated with very fast CMEs, which frequently are halos, whereas non-GLE-associated CMEs are significantly slower. We also found that the CME initial acceleration was by a factor 1.5 stronger for E $>$ 100 MeV events. For CMEs associated with GLE events, Gopalswamy et al. (2012) found the CME initial acceleration to be by a factor of 2 stronger than in ordinary CMEs. The ordinary CMEs of Gopalswamy et al. (2012) consisted of 448 limb CMEs with the average speed of 806 km s^{-1} and initial acceleration of 1 km s^{-2}. The GLE-associated CMEs had an average sky plane speed of 1885 km s^{-1} and initial acceleration of 2.3 km s^{-2}. Both

the average linear speeds (1017 and 1398 km s^{-1}) and the initial accelerations (1.35 and 1.96 km s^{-2}) of our E < 100 MeV and E > 100 MeV events are in qualitative agreement with Gopalswamy et al. (2012), results being in between of their ordinary and GLE-producing CMEs. Note that our E < 100 MeV events already have higher maximum energies than SEP events on average (Paassilta et al. 2017), and E > 100 MeV events include seven GLEs.

The average soft X-ray peak flux was significantly different (by a factor of 4) between E < 100 MeV and E > 100 MeV events (Table 1). The ranges were overlapping, but 59% of the E < 100 MeV events had SXR peak fluxes below $5.0 \cdot 10^{-5}$ W m^{-2}, whereas 77% of the E > 100 MeV had SXR peak fluxes above this limit. For GLEs in the time period 1986 – 2006, Firoz et al. (2011a) found that on average soft X-ray flares associated with GLE events were significantly stronger than non-GLE-associated flares. It is worth noting that the soft X-ray flare rise times were similar for the two groups of events. For the events of our dataset, the average SXR fluence was more than three times higher for E > 100 MeV events compared to E < 100 MeV events.

Firoz et al. (2019b) analyzed 14 GLE-associated and 23 non-GLE-associated SEP events occurring with soft X-ray flares of the size $\gtrsim$ M5. They found that the mean SXR fluence over the entire flare was by almost a factor two larger for the GLE-associated SEP events. Firoz et al. (2019b) also concluded that there was a strong linear dependence between the CME speed and the SXR fluence for the GLE-asociated SEP events (see also Andriopoulou et al. 2011), whereas the dependence was only weak in the non-GLE events. Similar trend is visible in our E > 100 MeV events (correlation coefficient $= 0.71 \pm 0.11$), whereas for E < 100 MeV, the correlation is weak (0.23 ± 0.14). In our dataset, all events with $F_i < 5.0 \cdot 10^{-4}$ J m^{-2} and CME speeds above 900 km s^{-1} were E < 100 MeV events. Also, events with CME speeds below 900 km s^{-1} at any F_i were very likely E < 100 MeV events. These values of V_{CME} and F_i define regions which contain most of the E < 100 MeV events and very few E > 100 MeV events. On the other hand, if the CME speed exceeds 1000 km s^{-1} and the X-ray peak flux is more than $5.0 \cdot 10^{-5}$ W m^{-2}, then with high probability the proton energies exceed 100 MeV.

All our events were associated with decametric-Type III radio bursts. All E > 100 MeV events and 91% of E < 100 MeV were associated with Type II bursts at metric or decametric–hectometric wavelengths. This is somewhat different from Kouloumvakos et al. (2015), who reported that Type III emission was associated with 53 out of 65 (82%) high-energy ($\sim$ 68 MeV) proton events and Type II emission with only 44 (68%) events. For E > 100 MeV events, both metric and DH-Type II bursts were observed in 88% of the events, whereas for E < 100 MeV, this association was only 50%. E < 100 MeV events were more frequently associated with metric-Type II bursts (25/32, 78%) than with DH-Type II (20/32, 63%). For E > 100 MeV events, these associations were almost equal (92% and 96%). Xie et al. (2016) found DH-Type II associations for all their 28 large, high-energy (> 10 MeV) proton events and m-Type II associations for 21 (75%) events.

Comparison of the release times of protons and SXR peak times showed that in most of the E < 100 MeV events (26/32, 81%), protons were released after the rise phase of the flare. The average time difference between the proton release time $t_{o,p}$ and the X-ray peak time t_{xrpk} was 18 ± 3 min. In a major part of the E > 100 MeV events (15/26, 58%), protons were released over the SXR flare rise phase with average time difference $t_{o,p} - t_{xrpk}$ of 4 ± 3 min. In general, protons in E < 100 MeV events are released later relative to the SXR flare onset time compared to E > 100 MeV events. This is in agreement with the investigation of Firoz et al. (2019a) of GLE-associated and non-GLE-associated SEP events.

Apart from one E > 100 MeV event, protons in both groups were released after the Type III radio burst onset, and with one exception in both groups after the metric-Type II onset. With respect to DH-Type II onsets, there was a clear difference between E < 100 MeV and E > 100 MeV events. Protons in 17 out of 20 (85%) E < 100 MeV events were released after the DH-Type II burst onset, whereas in most of the E > 100 MeV events (20/25, 80%), protons were released before the DH-Type II onset. Thus it appears that flares associated with low-coronal shocks manifested in m-Type II radio bursts dominate the high-energy protons (E > 100 MeV), whilst the CME propagation phases associated with shocks higher in the corona manifested in DH-Type II radio bursts dominate the lower-energy protons (E < 100 MeV) (see also Grechnev et al. 2015; Trottet et al. 2015; Firoz et al. 2019a,b; Zhang et al. 2022).

We examined the proton release heights and radio burst onset heights based on the CME heights at the particle release times and radio burst onset times. There was a significant overlap in the distributions of E < 100 MeV and E > 100 MeV events. The release heights of particles in E < 100 MeV events were in the range 1.5 – 9.8 $R_\odot$ with more than two thirds (21/31, 68%) at heights > 3.0 $R_\odot$. For E > 100 MeV events, the main range was from 1.0 $R_\odot$ to 5.4 $R_\odot$, with the majority (16/25, 64%) being at heights ≤ 3.0 $R_\odot$, but with two outliers at heights > 8 $R_\odot$. Similar release heights have been derived in other studies. For example, Kouloumvakos et al. (2015) estimated the release heights of their 65 high-energy proton events to be in the range from 1 $R_\odot$ to 8 $R_\odot$ with an average of 3.4 $R_\odot$. For GLE events, Reames (2009) found the particle release heights to be in the narrow range of 2 – 4 $R_\odot$ for well-connected events with increasing heights for events originating from the shock flanks. Gopalswamy et al. (2012) reported similar results for GLEs of Solar Cycle 23. The release heights ranged from 1.71 to 4.01 $R_\odot$ with an average of 3.09 $R_\odot$ for well-connected events and from 2.74 $R_\odot$ to 8.49 $R_\odot$ with an average of 5.18 $R_\odot$ for poorly connected events. Our results for E > 100 MeV events, which include seven GLE events, are in qualitative agreement with the results of Gopalswamy et al. (2012). Li et al. (2013) investigated the first GLE event of Solar Cycle 24 and concluded that the GLE protons were released when the associated CME was at the height ≈ 3.07 $R_\odot$. This is also in qualitative agreement with our result for the release heights of protons in E > 100 MeV events.

There was no significant difference in the onset heights of metric-Type II bursts in the two groups. Again, the situation was different for the radio bursts at decametric–hectometric wavelengths. For most of the E < 100 MeV events with DH-Type II emission (14/20, 70%), the onset heights were below 3.0 $R_\odot$, but mainly due to one event at exceptionally large height (6.4 $R_\odot$), the average was 3.0 ± 0.2 $R_\odot$. For most of the E > 100 MeV events (17/24, 71%), the onset heights were above 3.0 $R_\odot$ with the average of 4.4 ± 0.4 $R_\odot$. In general, we found that the average DH-Type II onset heights for E > 100 MeV events were higher than the average proton release heights, whereas they were lower for the E < 100 MeV events, as shown in Table 1. Comparison of the release times of particles and DH-Type II onset times showed that particles in most of the E < 100 MeV events were released after the DH-Type II onsets, whereas in 20 out of 25 (80%) E > 100 MeV events, they were released before the DH-Type II onset. This is in qualitative agreement with the results of Firoz et al. (2019a,b) and Zhang et al. (2022). Therefore it is likely that particles in the majority of E > 100 MeV events are accelerated either by the flare reconnection processes

or by shocks low in the corona. The nature of the exciter of the low-coronal shocks is not clear. For example, Grechnev et al. (2015) favors sharply erupting flux ropes instead of flare pressure pulses or the outer surface of CMEs. Protons in the E > 100 MeV events could undergo reacceleration higher in the corona in CME shocks observed as DH-Type II emission. Protons in E < 100 MeV events, again, are mainly accelerated in CME shocks at coronal heights > 3 $R_\odot$.

5. Conclusions

Based on our dataset of 32 E < 100 MeV events, in which proton energies extended up to ∼ 68 MeV but did not reach 100 MeV, and 26 E > 100 MeV events, in which energies exceeded 100 MeV, we defined limits for CME speed and soft X-ray peak flux or total fluence, which were used to make distinction between these two groups of events. If the CME speed is above 1000 $km\,s^{-1}$ and the X-ray peak flux is more than $5 \cdot 10^{-5}$ $W\,m^{-2}$, then with high probability protons exceed the energy of 100 MeV. On the other hand, in our dataset, all events with the X-ray total fluence below $5 \cdot 10^{-4}$ $J\,m^{-2}$ and CME speeds > 900 $km\,s^{-1}$ were E < 100 MeV events, and events with CME speeds below this limit with any X-ray total fluence very rarely had energies exceeding 100 MeV.

The observed higher proton peak intensities and rise rates emphasized at higher nominal energies (63.9 MeV vs. 17.5 MeV) and harder energy spectra of E > 100 MeV events demonstrate a more efficient acceleration mechanism involved in these events and rapidly decaying efficiency of the acceleration process in E < 100 MeV events.

The CMEs associated with E > 100 MeV events had on average significantly higher speeds and were more frequently halos compared to E < 100 MeV events, indicating association of SEP events reaching energies above 100 MeV with generally more energetic CMEs.

Protons in the E > 100 MeV events were mostly released low in the corona (≤ 3.0 $R_\odot$) before the onset of decametric–hectometric radio Type II bursts. Protons in the E < 100 MeV events, on the other hand, were mostly released higher in the corona (> 3 $R_\odot$) and after the DH-Type II onsets.

There was almost no difference in the rise time of the associated soft X-ray flares between the two groups of proton events, but the E > 100 MeV events had a tendency of being released over the rise phases of the SXR flares, whereas protons in E < 100 MeV events were released after the flare peaks.

We conclude that particles in the majority of E > 100 MeV events are accelerated either by the flare reconnection processes or by shocks low in the corona and could undergo reacceleration higher in the corona in CME shocks observed as DH-Type II emission. Protons in E < 100 MeV events, again, are mainly accelerated in CME shocks at coronal heights > 3 $R_\odot$.

Appendix A

Table 2 List of high-energy proton events with associated soft X-ray flares, CMEs, and radio emissions during 1996 – 2022.

N:o	High-energy proton events					Solar soft X-ray flares				CMEs		Radio emissions		
	Date	Release time	Path length	CA[a]	Group	Onset time[b]	Peak time	Class	Location	Time[c]	Speed[d]	t_{III}[e]	t_{mII}[e]	t_{DHII}[e]
	mm.dd.yyyy	UT	AU	°		UT	UT		°	UT	km s^{-1}	UT	UT	UT
1	24.09.1997	03.24 ± 0.12	1.52 ± 0.55	− 90	E < 100 MeV	02.43	02.48	M5.9	S31E19	03.38	532*	02.52	02.49	···
2	04.11.1997	06.16 ± 0.02	1.48 ± 0.05	− 46	E > 100 MeV	05.52	05.58	X2.1	S14W33	06.10	785	05.56	05.58	06.00
3	20.04.1998	10.47 ± 0.03	1.33 ± 0.09	23	E > 100 MeV	09.38	10.21	M1.4	S22W90	10.07	1863*	10.05	09.56	10.25
4	02.05.1998	13.52 ± 0.08	0.98 ± 0.22	− 26	E > 100 MeV	13.31	13.42	X1.1	S15W15	14.06	938	13.35	13.41	14.25
5	09.05.1998	03.52 ± 0.04	2.08 ± 0.12	54	E < 100 MeV	03.04	03.40	M7.7	???W100	03.36	2331*	03.22	03.26	03.35
6	22.11.1998	06.52 ± 0.05	1.34 ± 0.12	21	E < 100 MeV	06.30	06.42	X3.7	S27W82	DG	DG	06.41	06.38	···
7	09.05.1999	18.27 ± 0.04	0.98 ± 0.10	30	E < 100 MeV	17.53	18.07	M7.6	???W95	18.28	615*	17.59	···	···
8	18.01.2000	17.51 ± 0.08	1.79 ± 0.23	− 88	E < 100 MeV	17.07	17.27	M3.9	S19E11	17.54	739	17.12	···	17.31
9	17.02.2000	20.57 ± 0.03	1.31 ± 0.08	− 70	E < 100 MeV	20.17	20.35	M1.3	S29E07	21.30	728	20.29	20.25	20.42
10	02.03.2000	08.49 ± 0.02	1.30 ± 0.05	− 5	E < 100 MeV	08.20	08.28	X1.1	S14W52	08.54	776*	08.25	08.27	···
11	03.03.2000	02.22 ± 0.04	1.65 ± 0.10	1	E < 100 MeV	02.08	02.14	M3.8	S15W60	02.30	841*	02.12	02.12	···
12	04.04.2000	15.43 ± 0.06	0.95 ± 0.17	0	E < 100 MeV	15.12	15.41	C9.7	N16W66	16.33	1188	15.17	15.25	15.45
13	10.06.2000	17.10 ± 0.02	1.09 ± 0.05	− 10	E > 100 MeV	16.40	17.02	M5.2	N22W38	17.08	1108	16.56	16.55	17.15
14	18.06.2000	01.57 ± 0.06	1.80 ± 0.13	23	E < 100 MeV	01.52	01.59	X1.0	N23W85	02.10	629*	01.57	01.57	···
15	22.07.2000	11.27 ± 0.02	2.23 ± 0.03	− 2	E > 100 MeV	11.17	11.34	M3.7	N14W56	11.54	1230*	11.30	11.25	11.45
16	12.09.2000	12.45 ± 0.03	1.25 ± 0.06	− 58	E < 100 MeV	11.31	12.13	M1.0	S17W09	11.54	1550	11.46	11.33	12.00
17	24.11.2000	04.56 ± 0.06	2.86 ± 0.17	− 66	E > 100 MeV	04.55	05.02	X2.0	N20W06	05.30	1289	05.00	05.02	05.10
18	28.01.2001	16.06 ± 0.09	2.51 ± 0.26	− 16	E > 100 MeV	15.40	16.00	M1.5	S04W59	15.54	916	15.46	···	15.45
19	29.03.2001	10.49 ± 0.05	1.06 ± 0.16	− 29	E < 100 MeV	09.57	10.15	X1.7	N20W19	10.26	942	09.59	10.03	10.12
20	02.04.2001	12.12 ± 0.09	1.62 ± 0.20	19	E < 100 MeV	10.58	11.36	X1.1	N16W62	11.26	992	11.00	11.10	11.30
21	15.04.2001	13.40 ± 0.04	1.50 ± 0.14	33	E > 100 MeV	13.42*	13.50	X14	S20W85	14.07	1199*	13.39	13.47	14.05
22	20.05.2001	06.37 ± 0.06	1.02 ± 0.16	29	E > 100 MeV	06.00	06.03	M6.4	S17W91	06.26	546*	06.08	06.04	···

Table 2 (*Continued*)

N:o	High-energy proton events					Solar soft X-ray flares				CMEs		Radio emissions		
	Date	Release time	Path length	CA[a]	Group	Onset time[b]	Peak time	Class	Location	Time[c]	Speed[d]	t_{III}[e]	t_{mII}[e]	t_{DHII}[e]
	mm.dd.yyyy	UT	AU	°		UT	UT		°	UT	km s^{-1}	UT	UT	UT
23	04.06.2001	16.43 ± 0.07	1.35 ± 0.15	1	E < 100 MeV	16.21*	16.33	C3.2	N24W59	16.30	464*	16.22	16.14	···
24	24.09.2001	10.55 ± 0.04	1.39 ± 0.12	− 76	E > 100 MeV	10.15*	10.38	X2.6	S16E23	10.31	2402	10.18	···	10.45
25	19.10.2001	01.14 ± 0.08	2.50 ± 0.20	− 21	E < 100 MeV	00.47	01.05	X1.6	N16W18	01.27	558	01.03	00.59	01.15
26	22.10.2001	15.26 ± 0.03	1.27 ± 0.06	− 36	E > 100 MeV	14.27	15.08	M6.7	S21E18	15.06	1336	15.02	14.53	15.15
27	04.11.2001	16.24 ± 0.05	1.27 ± 0.15	− 62	E > 100 MeV	16.03	16.20	X1.0	N06W18	16.35	1810	16.12	16.10	16.30
28	22.11.2001	20.21 ± 0.05	1.98 ± 0.12	11	E > 100 MeV	20.18	20.36	M3.8	S25W67	20.31	1443	20.24	20.22	20.50
29	26.12.2001	05.23 ± 0.10	1.47 ± 0.29	− 10	E > 100 MeV	05:03*	05.40	M7.1	N08W54	05.30	1446*	05.13	04.59	05.20
30	20.02.2002	06.03 ± 0.03	1.08 ± 0.08	8	E < 100 MeV	06.06*	06.12	M5.1	N12W72	06.30	952	05.55	06.15	···
31	07.07.2002	11.51 ± 0.05	1.30 ± 0.09	21	E < 100 MeV	11.15	11.43	M1.0	???W95	11.31	1423*	11.17	···	11.35
32	18.08.2002	21.34 ± 0.10	1.84 ± 0.28	− 25	E < 100 MeV	21.12	21.25	M2.2	S12W19	21.54	682*	21.15	21.24	···
33	20.08.2002	08.27 ± 0.02	1.21 ± 0.05	− 15	E < 100 MeV	08.22	08.26	M3.4	S10W38	08.54	1099*	08.24	···	···
34	22.08.2002	02.13 ± 0.06	1.09 ± 0.17	1	E > 100 MeV	01.47	01.57	M5.4	S07W62	02.06	998	01.50	01.55	02.50
35	24.08.2002	00.58 ± 0.06	2.02 ± 0.24	14	E > 100 MeV	00.49	01.12	X3.1	S02W81	01.27	1913	00.51	01.01	01.45
36	09.11.2002	14.08 ± 0.16	1.51 ± 0.46	− 38	E < 100 MeV	13.08	13.23	M4.5	S12W29	13.32	1838	13.08	13.17	13.20
37	19.12.2002	22.03 ± 0.07	1.06 ± 0.16	− 39	E < 100 MeV	21.34	21.53	M2.7	N15W09	22.06	1092	21.41	21.39	21.45
38	23.04.2003	01.11 ± 0.03	1.51 ± 0.11	− 22	E < 100 MeV	00.58*	01.06	M5.1	N22W25	01.27	916*	01.03	01.01	···
39	31.05.2003	02.48 ± 0.07	1.04 ± 0.20	30	E > 100 MeV	02.13	02.24	M9.3	S07W65	02.30	1835	02.21	02.20	03.00
40	28.10.2003	10.52 ± 0.12	2.20 ± 0.40	− 43	E > 100 MeV	11.00*	11.10	X17	S16E08	11.30	2459	11.02	11.00	11.10
41	11.04.2004	04.42 ± 0.02	1.28 ± 0.05	− 13	E < 100 MeV	03.54	04.19	C9.6	S16W46	04.30	1645*	03.58	···	04.20
42	16.06.2005	20.21 ± 0.03	1.28 ± 0.07	50	E > 100 MeV	20.01	20.22	M4.0	N08W90	DG	DG	20.12	20.10	20.25

Table 2 (*Continued*)

N:o	High-energy proton events					Solar soft X-ray flares				CMEs		Radio emissions		
	Date	Release time	Path length	CA[a]	Group	Onset time[b]	Peak time	Class	Location	Time[c]	Speed[d]	t_{III}[e]	t_{mII}[e]	t_{DHII}[e]
	mm.dd.yyyy	UT	AU	°		UT	UT		°	UT	km s^{-1}	UT	UT	UT
43	14.08.2010	10.19 ± 0.03	1.12 ± 0.08	− 12	E < 100 MeV	09.38	10.05	C4.4	N17W52	10.12	1205	09.56	09.50	10.00
44	28.01.2011	01.33 ± 0.10	1.34 ± 0.33	5	E < 100 MeV	00.44	01.03	M1.3	N16W88	01.26	606*	01.04	01.02	01.15
45	07.03.2011	20.33 ± 0.07	1.81 ± 0.18	− 21	E < 100 MeV	19.43	20.12	M3.7	N30W48	20.00	2125	19.52	19.54	20.00
46	02.08.2011	06.35 ± 0.04	1.04 ± 0.12	− 36	E < 100 MeV	05.57*	06.19	M1.4	N14W15	06.36	712*	06.04	06.08	06.15
47	04.08.2011	04.12 ± 0.04	1.91 ± 0.12	− 39	E > 100 MeV	03.41	03.57	M9.3	N19W36	04.12	1315	03.52	03.54	04.15
48	08.08.2011	18.12 ± 0.04	1.27 ± 0.13	17	E < 100 MeV	18.00	18.10	M3.5	N16W61	18.12	1343*	18.04	18.07	18.10
49	09.08.2011	08.07 ± 0.04	0.96 ± 0.11	25	E > 100 MeV	07.48	08.05	X6.9	N17W69	08.12	1610	08.02	08.01	08.20
50	06.09.2011	02.10 ± 0.05	1.10 ± 0.13	− 58	E < 100 MeV	01.35	01.50	M5.3	N14W07	02.24	782	01.49	01.45	02.00
51	06.09.2011	22.28 ± 0.04	3.03 ± 0.13	− 44	E > 100 MeV	22.12	22.20	X2.1	N14W18	23.06	575	22.21	22.19	22.30
52	13.03.2012	17.28 ± 0.05	1.49 ± 0.16	21	E > 100 MeV	17.12	17.41	M7.9	N17W66	17.36	1884	17.21	17.15	17.35
53	20.02.2014	07.51 ± 0.03	1.17 ± 0.08	33	E > 100 MeV	07.38*	07.56	M3.0	S15W73	08.00	948	07.48	07.45	08.05
54	25.08.2014	16.05 ± 0.19	1.92 ± 0.50	− 51	E < 100 MeV	14.46	15.11	M2.0	N05W36	15.36	555	14.55	15.12	15.20
55	14.07.2017	02.26 ± 0.10	1.05 ± 0.34	− 39	E < 100 MeV	01.07	02.09	M2.4	S06W29	01.25	1200	01.21	⋯	01.18
56	06.09.2017	11.58 ± 0.05	2.16 ± 0.20	− 22	E > 100 MeV	11.53	12.02	X9.3	S08W33	12.24	1571	11.57	12.02	12.05
57	03.07.2021	14.59 ± 0.07	1.16 ± 0.21	19	E < 100 MeV	14.18	14.29	X1.5	N24W81	14.48	455*	14.30	⋯	⋯
58	28.10.2021	15.41 ± 0.06	1.92 ± 0.19	− 67	E > 100 MeV	15.17	15.35	X1.0	S26W05	15.48	1519	15.31	15.28	15.37

[a]CA = connection angle

[b]* Merged flares. The given onset time is for the flare considered to be associated with the particle event

[c]Time of the first appearance in LASCO C2

[d]* Nonhalo CME

[e]t_{III}, t_{mII}, and t_{DHII} refer to the onset times of decametric Type III, metric, and decametric–hectometric Type II, respectively. Ellipsis means that metric- or DH-Type II radio burst was not observed

Acknowledgments The authors would like to thank the anonymous reviewer for constructive comments and valuable suggestions. The authors gratefully acknowledge the various online data centers of NOAA and NASA. The LASCO CME catalog is generated and maintained by the Center for Solar Physics and Space Weather, The Catholic University of America, in cooperation with the Naval Research Laboratory and NASA. SOHO is a project of international cooperation between ESA and NASA.

Author contributions Dheyaa Ameri and Eino Valtonen wrote the main manuscript text. Rami Vainio and Amjad Al-Sawad reviewed the manuscript.

Funding Open Access funding provided by University of Turku (including Turku University Central Hospital). RV acknowledges support under ESA Contract No. 4000134036/21/D/MRP in the context of the Space Radiation Expert Service Centre and from the European Union's Horizon Europe programme under grant agreement No. 101135044 (SPEARHEAD). The European Commission is not responsible for any use that may be made of the information contained in this study.

Data Availability The list of analyzed events is available as a csv file on request.

Declarations

Competing interests The authors declare no competing interests.

References

Ameri, D., Valtonen, E., Pohjolainen, S.: 2019, Properties of high-energy solar particle events associated with solar radio emissions. *Solar Phys.* **294**, 122. DOI. ADS.

Andriopoulou, M., Mavromichalaki, H., Preka-Papadema, P., Plainaki, C., Belov, A., Eroshenko, E.: 2011, Solar activity and the associated ground level enhancements of solar cosmic rays during solar cycle 23. *Astrophys. Space Sci. Trans.* **7**, 439. DOI. ADS.

Bougeret, J.-L., Kaiser, M.L., Kellogg, P.J., Manning, R., Goetz, K., Monson, S.J., Monge, N., Friel, L., Meetre, C.A., Perche, C., Sitruk, L., Hoang, S.: 1995, Waves: the radio and plasma wave investigation on the wind spacecraft. *Space Sci. Rev.* **71**, 231. DOI. ADS.

Brueckner, G.E., Howard, R.A., Koomen, M.J., Korendyke, C.M., Michels, D.J., Moses, J.D., Socker, D.G., Dere, K.P., Lamy, P.L., Llebaria, A., Bout, M.V., Schwenn, R., Simnett, G.M., Bedford, D.K., Eyles, C.J.: 1995, The Large Angle Spectroscopic Coronagraph (LASCO). *Solar Phys.* **162**, 357. DOI. ADS.

Cane, H.V., Richardson, I.G., von Rosenvinge, T.T.: 2010, A study of solar energetic particle events of 1997 – 2006: their composition and associations. *J. Geophys. Res. Space Phys.* **115**, A08101. DOI. ADS.

Cliver, E.W., Kahler, S.W., Reames, D.V.: 2004, Coronal shocks and solar energetic proton events. *Astrophys. J.* **605**, 902. DOI. ADS.

Cliver, E.W., Ling, A.G.: 2009, Low-frequency type III bursts and solar energetic particle events. *Astrophys. J.* **690**, 598. DOI. ADS.

Desai, M., Giacalone, J.: 2016, Large gradual solar energetic particle events. *Living Rev. Solar Phys.* **13**, 3. DOI. ADS.

Domingo, V., Fleck, B., Poland, A.I.: 1995, The SOHO mission: an overview. *Solar Phys.* **162**, 1. DOI. ADS.

Firoz, K.A., Cho, K.-S., Hwang, J., Phani Kumar, D.V., Lee, J.J., Oh, S.Y., Kaushik, S.C., Kudela, K., Rybanský, M., Dorman, L.I.: 2010, Characteristics of ground-level enhancement-associated solar flares, coronal mass ejections, and solar energetic particles. *J. Geophys. Res. Space Phys.* **115**, A09105. DOI. ADS.

Firoz, K.A., Hwang, J., Dorotovič, I., Pintér, T., Kaushik, S.C.: 2011b, Relationship of ground level enhancements with solar, interplanetary and geophysical parameters. *Astrophys. Space Sci.* **331**, 469. DOI. ADS.

Firoz, K.A., Moon, Y.-J., Cho, K.-S., Hwang, J., Park, Y.D., Kudela, K., Dorman, L.I.: 2011a, On the relationship between ground level enhancement and solar flare. *J. Geophys. Res. Space Phys.* **116**, A04101. DOI. ADS.

Firoz, K.A., Gan, W.Q., Li, Y.P., Rodríguez-Pacheco, J., Kudela, K.: 2019a, On the possible mechanism of GLE initiation. *Astrophys. J.* **872**, 178. DOI. ADS.

Firoz, K.A., Gan, W.Q., Moon, Y.-J., Rodríguez-Pacheco, J., Li, Y.P.: 2019b, On the relation between flare and CME during GLE-SEP and non-GLE-SEP events. *Astrophys. J.* **883**, 91. DOI. ADS.

Gopalswamy, N.: 2003, Solar and geospace connections of energetic particle events. *Geophys. Res. Lett.* **30**, 8013. DOI. ADS.

Gopalswamy, N., Mäkelä, P., Yashiro, S.: 2019, A catalog of type II radio bursts observed by Wind/WAVES and their statistical properties. *Sun Geosph.* **14**, 111. DOI. ADS.

Gopalswamy, N., Yashiro, S., Michałek, G., Kaiser, M.L., Howard, R.A., Reames, D.V., Leske, R., von Rosenvinge, T.: 2002, Interacting coronal mass ejections and solar energetic particles. *Astrophys. J. Lett.* **572**, L103. DOI. ADS.

Gopalswamy, N., Aguilar-Rodriguez, E., Yashiro, S., Nunes, S., Kaiser, M.L., Howard, R.A.: 2005, Type II radio bursts and energetic solar eruptions. *J. Geophys. Res. Space Phys.* **110**, A12S07. DOI. ADS.

Gopalswamy, N., Yashiro, S., Michalek, G., Xie, H., Mäkelä, P., Vourlidas, A., Howard, R.A.: 2010, A catalog of halo coronal mass ejections from SOHO. *Sun Geosph.* **5**, 7. ADS.

Gopalswamy, N., Xie, H., Yashiro, S., Akiyama, S., Mäkelä, P., Usoskin, I.G.: 2012, Properties of ground level enhancement events and the associated solar eruptions during solar cycle 23. *Space Sci. Rev.* **171**, 23. DOI. ADS.

Gopalswamy, N., Xie, H., Akiyama, S., Mäkelä, P.A., Yashiro, S.: 2014, Major solar eruptions and high-energy particle events during solar cycle 24. *Earth Planets Space* **66**, 104. DOI. ADS.

Gopalswamy, N., Yashiro, S., Thakur, N., Mäkelä, P., Xie, H., Akiyama, S.: 2016, The 2012 July 23 backside eruption: an extreme energetic particle event? *Astrophys. J.* **833**, 216. DOI. ADS.

Grechnev, V.V., Kiselev, V.I., Meshalkina, N.S., Chertok, I.M.: 2015, Relations between microwave bursts and near-Earth high-energy proton enhancements and their origin. *Solar Phys.* **290**, 2827. DOI. ADS.

Huttunen-Heikinmaa, K., Valtonen, E., Laitinen, T.: 2005, Proton and helium release times in SEP events observed with SOHO/ERNE. *Astron. Astrophys.* **442**, 673. DOI. ADS.

Kahler, S., Ragot, B.R.: 2006, Near-relativistic electron c/v onset plots. *Astrophys. J.* **646**, 634. DOI. ADS.

Kallenrode, M.-B.: 2003, Current views on impulsive and gradual solar energetic particle events. *Sov. J. Nucl. Phys.* **29**, 965. ADS.

Kocharov, L., Torsti, J.: 2002, Hybrid solar energetic particle events observed on board Soho. *Solar Phys.* **207**, 149. DOI. ADS.

Kouloumvakos, A., Nindos, A., Valtonen, E., Alissandrakis, C.E., Malandraki, O., Tsitsipis, P., Kontogeorgos, A., Moussas, X., Hillaris, A.: 2015, Properties of solar energetic particle events inferred from their associated radio emission. *Astron. Astrophys.* **580**, A80. DOI. ADS.

Li, C., Firoz, K.A., Sun, L.P., Miroshnichenko, L.I.: 2013, Electron and proton acceleration during the first ground level enhancement event of solar cycle 24. *Astrophys. J.* **770**, 34. DOI. ADS.

Lintunen, J., Vainio, R.: 2004, Solar energetic particle event onset as analyzed from simulated data. *Astron. Astrophys.* **420**, 343. DOI. ADS.

Miroshnichenko, L.I.: 1996, Empirical model for the upper limit spectrum for solar cosmic rays at the Earth's orbit. *Radiat. Meas.* **26**, 421. DOI. ADS.

Miteva, R., Klein, K.-L., Samwel, S.W., Nindos, A., Kouloumvakos, A., Reid, H.: 2013, Radio signatures of solar energetic particles during the 23rd solar cycle. *Cent. Eur. Astrophys. Bull.* **37**, 541. DOI. ADS.

Paassilta, M., Raukunen, O., Vainio, R., Valtonen, E., Papaioannou, A., Siipola, R., Riihonen, E., Dierckxsens, M., Crosby, N., Malandraki, O., Heber, B., Klein, K.-L.: 2017, Catalogue of 55-80 MeV solar proton events extending through solar cycles 23 and 24. *J. Space Weather Space Clim.* **7**, A14. DOI. ADS.

Papaioannou, A., Sandberg, I., Anastasiadis, A., Kouloumvakos, A., Georgoulis, M.K., Tziotziou, K., Tsiropoula, G., Jiggens, P., Hilgers, A.: 2016, Solar flares, coronal mass ejections and solar energetic particle event characteristics. *J. Space Weather Space Clim.* **6**, A42. DOI. ADS.

Reames, D.V.: 1999, Particle acceleration at the Sun and in the heliosphere. *Space Sci. Rev.* **90**, 413. DOI. ADS.

Reames, D.V.: 2002, Magnetic topology of impulsive and gradual solar energetic particle events. *Astrophys. J. Lett.* **571**, L63. DOI. ADS.

Reames, D.V.: 2009, Solar release times of energetic particles in ground-level events. *Astrophys. J.* **693**, 812. DOI. ADS.

Reames, D.V.: 2013, The two sources of solar energetic particles. *Space Sci. Rev.* **175**, 53. DOI. ADS.

Reames, D.V.: 2021, *Solar Energetic Particles. A Modern Primer on Understanding Sources, Acceleration and Propagation*, *Lecture Notes in Physics* **978**. DOI. ADS.

Torsti, J., Valtonen, E., Lumme, M., Peltonen, P., Eronen, T., Louhola, M., Riihonen, E., Schultz, G., Teittinen, M., Ahola, K., Holmlund, C., Kelhä, V., Leppälä, K., Ruuska, P., Strömmer, E.: 1995, Energetic particle experiment ERNE. *Solar Phys.* **162**, 505. DOI. ADS.

Trottet, G., Samwel, S., Klein, K.-L., Dudok de Wit, T., Miteva, R.: 2015, Statistical evidence for contributions of flares and coronal mass ejections to major solar energetic particle events. *Solar Phys.* **290**, 819. DOI. ADS.

Vainio, R., Agueda, N., Aran, A., Lario, D.: 2007, In: Lilensten, J. (ed.) *Modeling of Solar Energetic Particles in Interplanetary Space* **27**, Springer, Dordrecht ISBN 978-1-4020-5446-4. DOI.

Vainio, R., Valtonen, E., Heber, B., Malandraki, O.E., Papaioannou, A., Klein, K.-L., Afanasiev, A., Agueda, N., Aurass, H., Battarbee, M., Braune, S., Dröge, W., Ganse, U., Hamadache, C., Heynderickx, D., Huttunen-Heikinmaa, K., Kiener, J., Kilian, P., Kopp, A., Kouloumvakos, A., Maisala, S., Mishev, A., Miteva, R., Nindos, A., Oittinen, T., Raukunen, O., Riihonen, E., Rodríguez-Gasén, R., Saloniemi, O., Sanahuja, B., Scherer, R., Spanier, F., Tatischeff, V., Tziotziou, K., Usoskin, I.G., Vilmer, N.: 2013, The first SEPServer event catalogue ~68-MeV solar proton events observed at 1 AU in 1996–2010. *J. Space Weather Space Clim.* **3**, A12. DOI. ADS.

Van Hollebeke, M.A.I., Ma Sung, L.S., McDonald, F.B.: 1975, The variation of solar proton energy spectra and size distribution with heliolongitude. *Solar Phys.* **41**, 189. DOI. ADS.

Williamson, J.H.: 1968, Least-squares fitting of a straight line. *Can. J. Phys.* **46**, 1845. DOI. ADS.

Xie, H., Ofman, L., Lawrence, G.: 2004, Cone model for halo CMEs: application to space weather forecasting. *J. Geophys. Res. Space Phys.* **109**, A03109. DOI. ADS.

Xie, H., Mäkelä, P., Gopalswamy, N., St. Cyr, O.C.: 2016, Energy dependence of SEP electron and proton onset times. *J. Geophys. Res. Space Phys.* **121**, 6168. DOI. ADS.

Xie, H., St. Cyr, O.C., Mäkelä, P., Gopalswamy, N.: 2019, Statistical study on multispacecraft widespread solar energetic particle events during solar cycle 24. *J. Geophys. Res. Space Phys.* **124**, 6384. DOI. ADS.

Yashiro, S., Gopalswamy, N., Michalek, G., St. Cyr, O.C., Plunkett, S.P., Rich, N.B., Howard, R.A.: 2004, A catalog of white light coronal mass ejections observed by the SOHO spacecraft. *J. Geophys. Res. Space Phys.* **109**, A07105. DOI. ADS.

York, D., Evensen, N.M., Martínez, M.L., De Basabe Delgado, J.: 2004, Unified equations for the slope, intercept, and standard errors of the best straight line. *Am. J. Phys.* **72**, 367. DOI. ADS.

Zhang, J., Dere, K.P.: 2006, A statistical study of main and residual accelerations of coronal mass ejections. *Astrophys. J.* **649**, 1100. DOI. ADS.

Zhang, J., Dere, K.P., Howard, R.A., Kundu, M.R., White, S.M.: 2001, On the temporal relationship between coronal mass ejections and flares. *Astrophys. J.* **559**, 452. DOI. ADS.

Zhang, Y., Firoz, K.A., Gan, W., Li, Y., Jia, H.: 2022, A study of the possible mechanism of the ground level enhancement on 28 October 2021. *Solar Phys.* **297**, 155. DOI. ADS.

Authors and Affiliations

Dheyaa Ameri[1,2] · Eino Valtonen[2] · Amjad Al-Sawad[3] · Rami Vainio[2]

✉ D. Ameri
dheyaa.abdulsada@uobasrah.edu.iq

E. Valtonen
eino.valtonen@utu.fi

A. Al-Sawad
dr.amjad@scrdiraq.gov.iq

R. Vainio
rami.vainio@utu.fi

1 Department of Ecology, College of Science, University of Basrah, Basrah, Iraq

2 Department of Physics and Astronomy, University of Turku, 20014 Turku, Finland

3 Ministry of Higher Education and Scientific Research, Baghdad, Iraq